Journal of Solid Mechanics Vol. 6, No. 3 (2014) pp. 265-277

Nonlinear Dynamic Buckling of Viscous-Fluid-Conveying PNC Cylindrical Shells with Core Resting on Visco-Pasternak Medium

A. Ghorbanpour Arani[1,2,*], A.A. Mosallaie Barzoki[1], R. Kolahchi[1]

[1]*Faculty of Mechanical Engineering, University of Kashan, Kashan , Islamic Republic of Iran*
[2]*Institute of Nanoscience & Nanotechnology, University of Kashan, Kashan, Islamic Republic of Iran*

Received 3 April 2014; accepted 4 June 2014

ABSTRACT

The use of intelligent nanocomposites in sensing and actuation applications has become quite common over the past decade. In this article, electro-thermo-mechanical nonlinear dynamic buckling of an orthotropic piezoelectric nanocomposite (PNC) cylindrical shell conveying viscous fluid is investigated. The composite cylindrical shell is made from Polyvinylidene Fluoride (PVDF) and reinforced by zigzag boron nitride nanotubes (BNNTs) where characteristics of the equivalent PNC being determined using micro-mechanical model. The poly ethylene (PE) foam-core is modeled based on Pasternak foundation. Employing the charge equation, Donnell's theory and Hamilton's principle, the four coupled nonlinear differential equations containing displacement and electric potential terms are derived. Harmonic differential quadrature method (HDQM) is applied to obtain the critical dynamic buckling load. A detailed parametric study is conducted to elucidate the influences of the geometrical aspect ratio, in-fill ratio of core, viscoelastic medium coefficients, material types of the shell and temperature gradient on the dynamic buckling load of the PNC cylindrical shell. Results indicate that the dimensionless critical dynamic buckling load increases when piezoelectric effect is considered.

Keywords: BNNTs; Nanocomposite; Cylindrical shell conveying viscous fluid; Nonlinear dynamic buckling response; HDQM

1 INTRODUCTION

BUCKLING of cylindrical shell under various loads has been significant in different industries and hereby is investigated by numerical researchers. Buckling strength of the cylindrical shell and tank subjected to axially compressive loads was illustrated by Kim and Kim [1] and they showed that the buckling strength of the shell and tank decreases significantly as the amplitude of initial geometric imperfection increases. Some researches about buckling are done by Ghorbanpour Arani et al. [2-3]. Buckling and ultimate strength criteria of stiffened shells under combined loading for reliability analysis were investigated by Das et al. [4]. The buckling of long steel cylindrical shells subjected to external pressure was studied by Hubner et al. [5]. They compared numerical analyses with test results from publications in some cases of a buckling ring. Linear and nonlinear dynamic stability of cylindrical shell is considered by some researchers. Buckling and dynamic instability analysis of stiffened shell panels was studied by Patel et al. [6]. They applied the method of Hill's infinite determinant to analyze the dynamic instability

* Corresponding author. Tel.: +98 31 55912450; Fax: +98 31 55912424.
E-mail address: aghorban@kashanu.ac.ir (A. Ghorbanpour Arani).

regions. After that nonlinear dynamic buckling of functionally graded cylindrical shells subjected to time-dependent axial load was considered by Huang and Han [7]. Their work was illustrated by various effects of the inhomogeneous parameter, loading speed, dimension parameter, environmental temperature rise and initial geometrical imperfection on nonlinear dynamic buckling.

Composites reinforced with nanotubes are new class of materials that applied in nano technology. These structures are used in airspace, oil and gas and other high technology industries. Dynamic buckling of fiber composite shells under impulsive axial compression was investigated by Bisagni [8]. He showed that with increasing the load duration, the dynamic buckling loads are decreased quickly and get significantly smaller than the static loads. Also he resulted that, since the common practice is to assume that dynamic bucking loads are higher than the static ones, which means that static design is safe, careful design is recommended. Nonlinear dynamic thermo-mechanical buckling analysis of the imperfect laminated and sandwich cylindrical shells based on a global-local theory inherently suitable for non-linear analyses was done by Shariyat [9]. He applied a novel three-dimensional high-order global-local theory to satisfy all the kinematic and the inter laminar stress continuity conditions at the layer interfaces. Effect of CNT length and CNT-matrix interphase in carbon CNT reinforced composites was investigated by Wan [10]. A micromechanics model was developed by Li and Saigal [11] for assessing the interfacial shear stress transfer in CNT reinforced composites. Many number of recent researches considered linear and nonlinear analysis of composite structure reinforced with nano tubes.

Most of these nonlinear researches are done with numerical methods such as (HDQM). Geometrically nonlinear analysis of laminated composite thin shells using a modified first-order shear deformable element-based Lagrangian shell element are investigated by Han at al. [12]. Nonlinear stability analysis of thin doubly curved orthotropic shallow shells by the differential quadrature method (DQM) was studied by Wang [13]. Dynamic analysis of composite cylindrical shells using DQM was illustrated by Haftchenari et al. [14]. Alibeigloo [15] considered static and vibration analysis of axi-symmetric angle-ply laminated cylindrical shell using state space DQM. He investigated the effect of edges condition on the static and vibration behavior of shell.

With respect to developmental works on buckling of the cylindrical shells, it should be noted that none of the research mentioned above, have considered smart composites and their specific characteristics. Recently, electro-thermo-mechanical torsional buckling of a piezoelectric polymeric cylindrical shell reinforced by BNNTs with an elastic core was investigated by Mosallaie Barzoki et al. [16]. They calculated the buckling load of the system based on Donnell theory and principle of minimum potential energy. Their results indicate that buckling strength increases substantially as harder foam cores are employed. After that, they [17] illustrated the nonlinear buckling response of embedded piezoelectric cylindrical shell reinforced with BNNT under electro–thermo-mechanical loadings using HDQM. Their results indicated critical buckling load increases when piezoelectric effect is considered.

However, in the present work for the first time, the effect of partially filled poly ethylene (PE) foam core on the behavior of an isotropic and clamped supported PVDF cylindrical shell reinforced by BNNTs is analyzed using energy method. Finally, four coupled nonlinear equation are obtained and solved with HDQM in order to obtain the dynamic buckling load of the smart nanocomposite. The effects of geometrical aspect ratio, in-fill ratio of core, viscoelastic medium coefficients, material types of the shell and temperature gradient on the dynamic buckling load of the PNC cylindrical shell have been taken into account.

2 BASIC EQUATIONS

Fig. 1 shows a piezoelectric cylindrical shell reinforced with BNNTs embedded in a viscoelastic foundation which is simulated with spring constant of Winkler-type and shear constant of Pasternak-type as well as damping coefficient. Also, the radiuses of the shell and core are illustrated with R and length R_c, respectively.

Constitutive equations are expressed in electro-thermo-mechanical coupled form, because the BNNTs and PVDF have piezoelectricity characteristics. In fact, any changes in mechanical strain leads to change in electrical field and vice versa. In piezoelectric materials, the constitutive equations may be arbitrarily combined as follows [18-20]:

$$\begin{Bmatrix} \sigma_{xx} \\ \sigma_{\theta\theta} \\ \sigma_{x\theta} \\ D_{xx} \end{Bmatrix} = \begin{bmatrix} C_{11} & C_{12} & 0 & -e_{11} \\ C_{12} & C_{22} & 0 & 0 \\ 0 & 0 & C_{66} & 0 \\ e_{11} & 0 & 0 & \in_{11} \end{bmatrix} \begin{Bmatrix} \varepsilon_{xx} - \alpha_{xx}\ \Delta T \\ \varepsilon_{\theta\theta} - \alpha_{\theta\theta}\ \Delta T \\ 2\varepsilon_{x\theta} \\ E_{xx} \end{Bmatrix}, \tag{1}$$

where σ, ε, D and E are stress, strain, electric displacement and electric field tensors, respectively. Also, C_{ij}, e_{ij}, $\in_{ii}$ $(i,j=1,...6)$ are elastic, piezoelectric and dielectric constants, respectively which can be obtained by micromechanical model for PNC [14], and α_{kk} $(k=x,\theta)$, ΔT and E_{xx} representing respectively, thermal expansion coefficient, thermal gradient and electric field which the latter is defined as a function of electric potential, ϕ_{xx} as below:

$$E_{xx}=-\frac{\partial\phi_{xx}}{\partial x}. \tag{2}$$

Based on Kirchhoff-Law assumptions, the displacement components of an arbitrary point may be written as [21]:

$$\mathrm{u}(x,\theta,z)=u_0(x,\theta)-z\frac{\partial w(x,\theta)}{\partial x},\mathrm{v}(x,\theta,z)=v_0(x,\theta)-\frac{z}{R}\frac{\partial w(x,\theta)}{\partial\theta},w(x,\theta,z)=w(x,\theta). \tag{3}$$

Using Donnell's theory, strains may be obtained by a combination of linear, nonlinear and curvature change terms as:

$$\varepsilon_{xx}=u_{,x}+\frac{1}{2}w_{,x}{}^2-zw_{,xx},\varepsilon_{\theta\theta}=\frac{v_{,\theta}}{R}+\frac{w}{R}+\frac{1}{2R^2}w_{,\theta}{}^2-\frac{z}{R^2}w_{,\theta\theta},2\varepsilon_{x\theta}=\frac{u_{,\theta}}{R}+v_{,x}+\frac{w_{,x}w_{,\theta}}{R}-\frac{2z}{R}w_{,x\theta}, \tag{4}$$

where x and θ denote axial and circumferential direction of coordinate system, respectively, z is the distance from an arbitrary point to the middle surface.

The total potential energy, V, of the piezoelectric polymeric cylindrical shell conveying fluid is the sum of strain energy, U, kinetic, K, and the work done by the viscoelastic medium and fluid, W. Considering the governing (i.e. Eq. (1)) and strain displacement Eq. (4), and assuming longitudinally polarized PVDF (i.e. $E_\theta=E_z=0$), U and K may be expressed as [16]:

$$\begin{aligned}U=\int_{-\frac{h}{2}}^{\frac{h}{2}}\iint_A\Bigg(&\sigma_{xx}\left(\frac{\partial u}{\partial x}+\frac{1}{2}\left(\frac{\partial w}{\partial x}\right)^2-z\frac{\partial^2 w}{\partial x^2}\right)+\sigma_{\theta\theta}\left(\frac{\partial v}{R\partial\theta}+\frac{w}{R}+\frac{1}{2}\left(\frac{\partial w}{R\partial\theta}\right)^2-z\frac{\partial^2 w}{R^2\,\partial\theta^2}\right)\\&+\sigma_{x\theta}\left(\frac{\partial u}{R\partial\theta}+\frac{\partial v}{\partial x}+\frac{\partial w}{R\partial\theta}\frac{\partial w}{\partial x}-2z\frac{\partial^2 w}{R\partial\theta\,\partial x}\right)+D_x\frac{\partial\phi}{\partial x}\Bigg)dA\,dz,\end{aligned} \tag{5}$$

where dA is cross section element. The Kinetic energy can be written as:

$$K=\frac{\rho}{2}\iint_A\left(\frac{\partial u}{\partial t}\right)^2+\left(\frac{\partial v}{\partial t}\right)^2+\left(\frac{\partial w}{\partial t}\right)^2dz\,dA, \tag{6}$$

where ρ is density of nano composite cylinder. The work done by the viscoelastic medium and fluid can be expressed as:

$$W=-\int\left(F_{fluid}+F_{ve}\right)wdA, \tag{7}$$

where F_{vs} and F_{fluid} are the applied force by viscoelastic and fluid, respectively. According to Navier-Stoks equation for viscous incompressible, we have:

$$\rho_f \frac{dV}{dt} = -\nabla \mathrm{P} + \mu \nabla^2 \mathrm{V} + \mathrm{F}_{body}, \tag{8}$$

where ρ_f, μ, F_{body}, V and P are density, viscosity, body forces, speed and pressure of fluid , respectively. Furthermore, ∇ and ∇^2 are gradient and Laplasian operators, respectively and $\frac{d}{dt}$ is perfect derivative which can be defined as below:

$$\frac{d}{dt} = \frac{\partial}{\partial t} + v_x \frac{\partial}{\partial x} + v_\theta \frac{\partial}{\partial \theta} + v_z \frac{\partial}{\partial z}, \tag{9}$$

where t is time. Substituting Eq. (9) into Eq. (8) and neglecting the action of the body forces, yields to F_{fluid} as:

$$F_{fluid} = \int \left(-\rho_f \left(\frac{\partial^2 w}{\partial t^2} + 2v_x \frac{\partial^2 w}{\partial x\, \partial t} + {v_x}^2 \frac{\partial^2 w}{\partial x^2} \right) + \mu \left(\frac{\partial^3 w}{\partial x^2\, \partial t} + \frac{\partial^3 w}{R^2\, \partial \theta^2\, \partial t} + v_x \left(\frac{\partial^3 w}{\partial x^3} + \frac{\partial^3 w}{R^2\, \partial \theta^2\, \partial x} \right) \right) \right) w dA, \tag{10}$$

In addition, the work due to viscoelastic foundation can be expressed as:

$$F_e = k_W w - k_g \nabla^2 w + C\dot{w}, \tag{11}$$

where k_W, k_g and c_v are normal type of Winkler, shear type of Pasternak and dapping coefficient, respectively. The dimensionless parameters are defined as:

$$\begin{gathered}
\gamma_s = \frac{h_s}{L},\ \gamma_c = \frac{h_c}{L},\ \xi = \frac{x}{L},\ \beta_s = \frac{h_s}{R},\ \beta_c = \frac{h_c}{R}, \eta = \frac{R_c}{R},\ \{\bar{u}, \bar{v}, \bar{w}\} = \frac{\{u_1, v_1, w_1\}}{h_s} \bar{C}_{kij} = \frac{C_{kij}}{C_{s11}}, i, j = 1, 2, 6\ \ k = c, s \\
\bar{t} = \frac{t}{h_s \sqrt{\frac{\rho_f}{C_{s11}}}},\ C = \frac{h_s c_v}{\sqrt{C_{s11} \rho_f}},\ K_w = \frac{h_s k_w}{C_{s11}}, K_g = \frac{k_g}{h_s C_{s11}}, \Phi = \frac{\varphi_1}{\Phi_0},\ \Phi_0 = h_s \sqrt{\frac{C_{s11}}{\in_{11}}},\quad \bar{e}_{k11} = \frac{e_{k11}}{\sqrt{C_{s11} \in_{11}}},\quad k = c, s \\
\bar{\rho}_k = \frac{\rho_k}{\rho_f},\ k = c, s\ \ \bar{\mu} = \frac{\mu}{h_s \sqrt{C_{s11} \rho_f}},\quad V = v_x \sqrt{\frac{\rho_f}{C_{s11}}}\ \ N^*_{x0} = \frac{N_{x0}}{l C_{s11}}
\end{gathered} \tag{12}$$

where h_c and h_s are thickness of core and shell, respectively. Applying Hamilton principle ($\delta \int_0^t (K - U + W) dt = 0 \Rightarrow \int_0^t (\delta K - \delta U + \delta W) dt = 0$), integrating by parts and setting the coefficient of mechanical displacement and electric potential to zero lead to the following four coupled dimensionless equations:

$$\begin{gathered}
(\gamma_c \gamma_s \bar{C}_{c11} + \gamma_s^2) \left(\frac{\partial^2 \bar{u}}{\partial \xi^2} + \frac{\partial \bar{w}}{\partial \xi} \frac{\partial^2 \bar{w}}{\partial \xi^2} \right) + \frac{\beta_c \gamma_s \bar{C}_{c12}}{\eta} \left(\frac{\partial^2 \bar{v}}{\partial \xi \partial \theta} + \frac{\partial \bar{w}}{\partial \xi} + \frac{\partial \bar{w}}{\partial \theta} \frac{\beta_c}{\eta} \frac{\partial^2 \bar{w}}{\partial \xi \partial \theta} \right) \\
+ \gamma_s \beta_s \bar{C}_{s12} \left(\frac{\partial^2 \bar{v}}{\partial \xi \partial \theta} + \frac{\partial \bar{w}}{\partial \xi} + \beta_s \frac{\partial \bar{w}}{\partial \theta} \frac{\partial^2 \bar{w}}{\partial \xi \partial \theta} \right) + \frac{\beta_c \gamma_s \bar{C}_{c66}}{\eta} \left(\frac{\beta_c}{\eta} \frac{\partial^2 \bar{u}}{\partial \theta^2} + \frac{\partial^2 \bar{v}}{\partial \xi \partial \theta} + \frac{\beta_c}{\eta} \frac{\partial \bar{w}}{\partial \xi} \frac{\partial^2 \bar{w}}{\partial \theta^2} + \frac{\partial \bar{w}}{\partial \xi} + \frac{\beta_c}{\eta} \frac{\partial \bar{w}}{\partial \theta} \frac{\partial^2 \bar{w}}{\partial \xi \partial \theta} \right) \\
+ \beta_s \bar{C}_{s66} \left(\beta_s \frac{\partial^2 \bar{u}}{\partial \theta^2} + \frac{\partial^2 \bar{v}}{\partial \xi \partial \theta} + \beta_s \frac{\partial \bar{w}}{\partial \xi} \frac{\partial^2 \bar{w}}{\partial \theta^2} + \frac{\partial \bar{w}}{\partial \xi} + \beta_s \frac{\partial \bar{w}}{\partial \theta} \frac{\partial^2 \bar{w}}{\partial \xi \partial \theta} \right) + \gamma_c \gamma_s \bar{e}_{c11} \frac{\partial^2 \Phi}{\partial \xi^2} = C \frac{\partial \bar{u}}{\partial \bar{t}} + \left(\bar{\rho}_c \frac{\beta_c}{\beta_s} + \bar{\rho}_s \right) \frac{\partial^2 \bar{u}}{\partial \bar{t}^2},
\end{gathered} \tag{13}$$

$$\frac{\beta_c \bar{C}_{c12}}{\eta}\left(\frac{\partial^2 \bar{u}}{\partial\xi\,\partial\theta}+\frac{\partial \bar{w}}{\partial\xi}\frac{\partial^2 \bar{w}}{\partial\xi\partial\theta}\right)+\beta_s \bar{C}_{s12}\left(\frac{\partial^2 \bar{u}}{\partial\xi\partial\theta}+\frac{\partial \bar{w}}{\partial\xi}\frac{\partial^2 \bar{w}}{\partial\xi\partial\theta}\right)+\frac{\beta_c \beta_s \bar{C}_{c22}}{\eta^2}\left(\frac{\partial^2 v}{\partial\theta^2}+\frac{\partial \bar{w}}{\partial\theta}+\frac{\beta_c}{\eta}\frac{\partial \bar{w}}{\partial\theta}\frac{\partial^2 \bar{w}}{\partial\theta^2}\right)+$$
$$\beta_s^2 \bar{C}_{s22}\left(\frac{\partial^2 \bar{v}}{\partial\theta^2}+\frac{\partial \bar{w}}{\partial\theta}+\beta_s\frac{\partial \bar{w}}{\partial\theta}\frac{\partial^2 \bar{w}}{\partial\theta^2}\right)+\gamma_c \bar{C}_{c66}\left(\frac{\beta_c}{\eta}\frac{\partial^2 \bar{u}}{\partial\xi\partial\theta}+\frac{\partial^2 \bar{v}}{\partial\xi^2}+\frac{\beta_c}{\eta}\frac{\partial^2 \bar{w}}{\partial\theta\,\partial\xi}\frac{\partial \bar{w}}{\partial\xi}+\frac{\beta_c}{\eta}\frac{\partial \bar{w}}{\partial\theta}\frac{\partial^2 \bar{w}}{\partial\xi^2}\right)+ \quad (14)$$
$$\gamma_s \bar{C}_{s66}\left(\frac{\beta_s \partial^2 \bar{u}}{\partial\xi\partial\theta}+\frac{\partial^2 \bar{v}}{\partial\xi^2}+\frac{\beta_s \partial^2 \bar{w}}{\partial\theta\,\partial\xi}\frac{\partial \bar{w}}{\partial\xi}+\frac{\beta_s \partial \bar{w}}{\partial\theta}\frac{\partial^2 \bar{w}}{\partial\xi^2}\right)=\bar{C}\frac{\partial v}{\partial\bar{t}}+\left(\bar{\rho}_c\frac{\beta_c}{\beta_s}+\bar{\rho}_s\right)\frac{\partial^2 \bar{v}}{\partial\bar{t}^2},$$

$$\frac{\gamma_s^2}{12}\left(-\gamma_s^2\frac{\partial^4 \bar{w}}{\partial\xi^4}-\bar{C}_{s12}\beta_s^2\frac{\partial^4 \bar{w}}{\partial\xi^2\partial\theta^2}\right)+\frac{1}{12}\left(-\gamma_s^2\beta_s^2\bar{C}_{s12}\frac{\partial^4 \bar{w}}{\partial\xi^2\partial\theta^2}-\beta_s^4\bar{C}_{s22}\frac{\partial^4 \bar{w}}{\partial\theta^4}\right)-\frac{\gamma_s^2\beta_s^2\bar{C}_{c66}}{3}\left(\frac{\partial^4 \bar{w}}{\partial\xi^2\partial\theta^2}\right)$$
$$-\left(\frac{\gamma_c\beta_c C_{c12}}{3\eta}+\frac{\gamma_s\beta_s\bar{C}_{s12}}{3}\right)\left(\frac{\partial \bar{u}}{\partial\xi}+\frac{\gamma_s}{2}\left(\frac{\partial \bar{w}}{\partial\xi}\right)^2\right)-\left(\frac{\gamma_c\beta_c\bar{C}_{c22}}{\eta}\right)\left(\frac{\partial \bar{v}}{\partial\theta}+\frac{\gamma_s\bar{w}}{\eta}+\frac{1}{2}\frac{\beta_s^2}{\eta^2}\left(\frac{\partial \bar{w}}{\partial\theta}\right)^2\right)$$
$$-\beta_s\bar{C}_{s22}\left(\frac{\partial \bar{v}}{\partial\theta}+\beta_s\bar{w}+\frac{\beta_s^2}{2}\left(\frac{\partial \bar{w}}{\partial\theta}\right)^2\right)-\frac{\beta_c\bar{C}_{c22}}{\eta}\left(\frac{\partial \bar{v}}{\partial\theta}+\frac{\beta_s\bar{w}}{\eta}+\frac{\beta_s^2}{2\eta^2}\left(\frac{\partial \bar{w}}{R_c\,\partial\theta}\right)^2\right)$$
$$-\left(\left(\beta_s^2\alpha_{xs}+\frac{\beta_s\beta_c\bar{C}_{c11}\alpha_{xc}}{\eta^2}+\beta_s^2\bar{C}_{s12}\alpha_{\theta s}+\frac{\beta_s\beta_c\bar{C}_{c12}\alpha_{\theta c}}{\eta^2}\right)\frac{\partial^2 \bar{w}}{\partial\theta^2}\Delta T\right. \quad (15)$$
$$\left.-\left(\gamma_s^2\alpha_{xs}+\gamma_c\gamma_s\bar{C}_{c11}\alpha_{xc}+\gamma_s^2\bar{C}_{s12}\alpha_{\theta s}+\gamma_c\gamma_s\bar{C}_{c12}\alpha_{\theta c}\right)\frac{\partial^2 \bar{w}}{\partial\xi^2}\right)\Delta T$$
$$-\left[\frac{\beta_c}{\beta_s}\frac{\partial^2 \bar{w}}{\partial\bar{t}^2}+2\gamma_c V\frac{\partial^2 \bar{w}}{\partial\xi\partial\bar{t}}+\gamma_c\gamma_s V^2\frac{\partial^2 \bar{w}}{\partial\xi^2}\right]-\mu\left[\gamma_c\gamma_s\frac{\partial^3 \bar{w}}{\partial\xi^2\partial\bar{t}}+V\gamma_s^2\gamma_c\frac{\partial^3 \bar{w}}{\partial\xi^3}+\frac{\beta_s\beta_c}{\eta^2}\left(\frac{\partial^3 \bar{w}}{\partial\theta^2\partial\bar{t}}+V\gamma_s\frac{\partial^3 \bar{w}}{\partial\theta^2\partial\xi}\right)\right]$$
$$+\left(K_{ws}+K_{wc}\right)\bar{w}-\left(K_{gs}+K_{gc}\right)\left(\gamma_s^2\frac{\partial^2 \bar{w}}{\partial\xi^2}+\beta_s^2\frac{\partial^2 \bar{w}}{\partial\theta^2}\right)+\gamma_s N_{x0}^*\frac{\partial^2 \bar{w}}{\partial\xi^2}=\bar{C}\frac{\partial \bar{w}}{\partial\bar{t}}+\left(\bar{\rho}_c\frac{\beta_c}{\beta_s}+\bar{\rho}_s\right)\frac{\partial^2 \bar{w}}{\partial\bar{t}^2}.,$$

$$\frac{\partial^2\Phi}{\partial\xi^2}+\left(\bar{e}_{c11}\right)\left(\frac{\partial^2 \bar{u}}{\partial\xi^2}+\gamma_c\frac{\partial \bar{w}}{\partial\xi}\frac{\partial^2 \bar{w}}{\partial\xi^2}\right)=0. \quad (16)$$

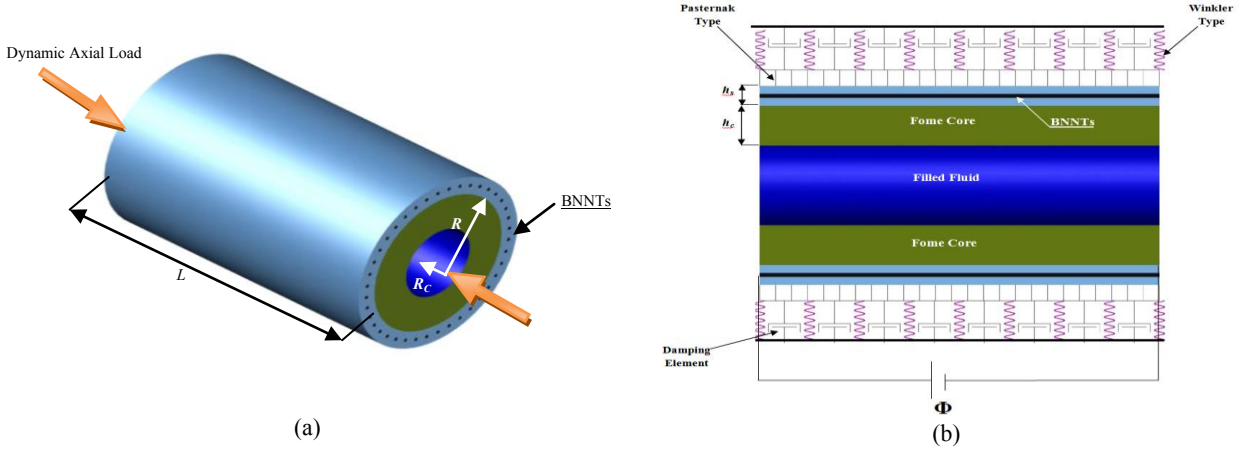

Fig. 1
a) Geometrical 3D view of nano composite cylindrical shell reinforced by BNNTs. B) Cut view of nano composite cylindrical shell conveying viscous fluid embedded in a visco-elastic medium.

3 HDQM

These four governing equations (Eqs. (13)–(16)) are discetized using HDQM, so that they are solved considering the associated boundary conditions to obtain vibration and instability of the viscose-fluid-conveying cylindrical shell made from PVDF. The HDQM approximates the partial derivative of a function F (representing $\overline{u}$, $\overline{v}$, $\overline{w}$ and Φ), with respect to two spatial variables (ξ and θ) at a given discrete point (ξ_i, θ_i), as a weighted linear sum of the function values at all discrete points chosen in the solution domain ($0 < \xi < L$, $0 < \theta < 2\pi$) with $N_\xi \times N_\theta$ grid points along ξ and θ axes, respectively. Then, the nth-order partial derivative of $F(\xi,\theta)$ with respect to ξ , the mth-order partial derivative of $F(\xi,\theta)$ with respect to θ and the (n + m)th-order partial derivative of $F(\xi,\theta)$ with respect to both ξ and θ is expressed discretely at the point (ξ_i, θ_i) as [17, 22, 23]:

$$\frac{d^n F(\xi_i,\theta_j)}{d\xi^n} = \sum_{k=1}^{N_\xi} A_{ik}^{(n)} F(\xi_k,\theta_j) \qquad n = 1,...,N_\xi - 1, \tag{17}$$

$$\frac{d^m F(\xi_i,\theta_j)}{d\theta^m} = \sum_{l=1}^{N_\theta} B_{jl}^{(m)} F(\xi_i,\theta_l) \qquad m = 1,...,N_\theta - 1, \tag{18}$$

$$\frac{d^{n+m} F(\xi_i,\theta_j)}{d\xi^n d\theta^m} = \sum_{k=1}^{N_\xi}\sum_{l=1}^{N_\theta} A_{ik}^{(n)} B_{jl}^{(m)} F(\xi_k,\theta_l), \tag{19}$$

where $A_{ik}^{(n)}$ and $B_{jl}^{(m)}$ are the weighting coefficients associated with n^{th}-order partial derivative of $F(\xi,\theta)$ with respect to ξ at the discrete point ξ_i and m^{th}-order derivative with respect to θ at θ_i, respectively, whose recursive formulae can be found in [23].

The associated mechanical clamped and free electrical boundary conditions at both ends of the shell, in HDQM form, may be written in dimensionless form as:

$$\begin{cases} \overline{w}_{i1} = \overline{v}_{i1} = \overline{u}_{i1} = \Phi_{i1} = 0, & \sum_{j=1}^{N_\theta} A_{2j}\overline{w}_{ji} = 0 \\ \overline{w}_{N_x i} = \overline{v}_{N_x i} = \overline{u}_{N_x i} = \Phi_{N_x i} = 0, & \sum_{j=1}^{N_\theta} A_{(N_x-1)j}\overline{w}_{ji} = 0 \end{cases} \quad for \quad i = 1...N_\theta. \tag{20}$$

Applying these boundary conditions into the above four governing equations, Eqs. (13)-(16), results governing equations in HDQM form as shown in Appendix A. Rearranged governing equations in matrix form yields:

$$[M]\{\ddot{q}\} - [C]\{\dot{q}\} + \left[[K] - \left(N_{xSt}^* + \alpha N_{xDy}^* \cos(\Omega\bar{t})\right)[K_G]\right]\{q\} = 0, \tag{21}$$

where [M], [C], [K], [K_G] are mass, viscose, stiffness and geometric stiffness matrixes, respectively. N_{xSt}^* is the static component of dimensionless harmonic axial load, N_{xDy}^* is its dynamic component and α is the coefficient of dynamic load. Furthermore, q can be expressed as:

$$\begin{aligned} \{d^b\} &= \{\overline{u}_{i1}, \overline{v}_{i1}, \overline{w}_{i1}, \overline{w}_{i2}, \Phi_{i1}, \overline{u}_{iN_\theta}, \overline{v}_{iN_\theta}, \overline{w}_{iN_\theta}, \overline{w}_{i(N_\theta-1)}, \Phi_{iN_\theta}\} \quad i = 1,...,N_x, \\ \{d^d\} &= \{\overline{u}_{ij}, \overline{v}_{ij}, \overline{w}_{i(j+1)}, \Phi_{ij}\} \qquad\qquad\qquad\qquad\qquad\qquad j = 2,...,N_x - 1. \end{aligned} \tag{22}$$

In the above equation, subscript b denotes boundary points and other points are indicated by subscript d . Finally, applying the boundary conditions into Eq. (21) yields the dynamic buckling load.

4 NUMERICAL RESULTS AND DISCUSSION

A circular embedded PNC cylindrical shell with a foam core, which is assumed to have the length, $L = 0.2\ m$, length to shell radius ratio, $L/R = 2$, shell thickness to shell radius ratio, $h_s/R = 0.01$, core radius to shell radius ratio, $R_c/R = 0.5$. The applied forces on the PNC are combination of fluid pressure, elastic foundation and axial dynamic harmonic force where the latter is time depended. In order to obtain the nonlinear dynamic critical buckling load (N_{Dy}^{cr*}) for PNC cylindrical shell, HDQM is used in conjunction with a program being written in MATLAB. The effects of dimensionless parameters such as aspect ratios of thickness to radius of the shell, (β_s), in-fill ratio of core η (corresponding to the thickness of the foam core), aspect ratios of thickness to length of the shell, (γ_s), Winkler, (K_W) and Pasternak,(K_g) modules as well as the material types of the shell for illustrating piezoelectricity influence and temperature gradient, (ΔT), were investigated. Mechanical, electrical and thermal characteristics of PVDF matrix, BNNTs reinforce, and PE foam core are presented in Table 1. [16]. It should be noted that in the following figures, the dimensionless fluid velocity is considered $V = 0.1$ [21].

Figs. 2 and 3 demonstrate the effects of geometrical aspect ratio on the critical dynamic buckling load (N_{Dy}^{cr*}) versus dimensionless maximum transverse displacement ($W_{\max}/h_s$). It should be noted that in Figs. 2 and 3 the aspect ratio is defined as thickness to length of the shell (γ_s) and thickness to radius of shell (β_s), respectively. It is obvious that without static terms, with increasing the dynamic buckling load, $W_{\max}/h_s$ is equal to zero because buckling didn't occur. In specific value of it, suddenly $W_{\max}/h_s$ is started to increase with very sharply rate. This value might be critical dynamic buckling load. As can be seen, changing aspect ratios has a significant effect on dynamic buckling load of the system. Increasing β_s and γ_s leads to increase system stiffness and, however, dynamic critical buckling load is increased and transverse deflection is decreased. Difference between two geometrical aspect ratios is in amount of N_{Dy}^{cr*}. Waxing of γ_s have more effect on amount of dynamic buckling than β_s but its effect on changing of $W_{\max}/h_s$ is less than β_s. Fig. 4 illustrates the effect of foam core thickness (η) on dynamic nonlinear buckling load. It can be found that the N_{Dy}^{cr*} is decreased with increasing η, because stiffness of system is gotten more with increasing foam core thickness. Furthermore, for the cases of shell without any foam core (i.e. $\eta = 1$) such as pipes conveying viscous fluid and shell with full foam core (i.e. $\eta = 0$), the N_{Dy}^{cr*} is minimum and maximum, respectively.

Table 1
Mechanical, electrical, and thermal properties of PVDF, BNNT and PE.

PVDF	BNNT	PE
$C_{11} = 238.24(\text{GPa})$	$E = 1.8(\text{TPa})$	$E = 125(\text{GPa})$
$C_{22} = 23.6(\text{GPa})$	$\upsilon = 0.34$	$\upsilon = 0.30$
$C_{12} = 3.98(\text{GPa})$	$e_{11} = 0.95(\text{C/ m}^2)$	$\rho = 1.45(\text{kg/ m}^3)$
$C_{66} = 6.43(\text{GPa})$	$\alpha_x = 1.2\times10^{-6}(1/\text{K})$	
$e_{11} = -0.135(\text{C/ m}^2)$	$\alpha_\theta = 0.6\times10^{-6}(1/\text{K})$	
$e_{12} = -0.145(\text{C/ m}^2)$		
$\in = 1.1068\times10^{-8}(\text{F/ m})$		
$\alpha_x = 7.1\times10^{-5}(1/\text{K})$		
$\alpha_\theta = 7.1\times10^{-5}(1/\text{K})$		

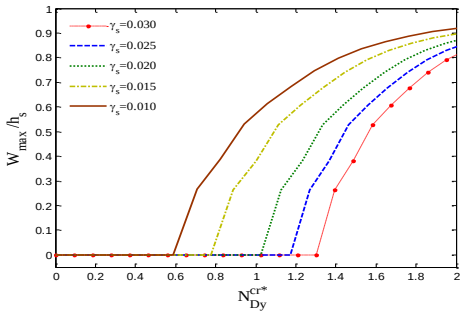

Fig. 2
Effect of shell length aspect ratio (γ_s) on the nonlinear dynamic critical buckling load versus dimensionless transverse displacement.

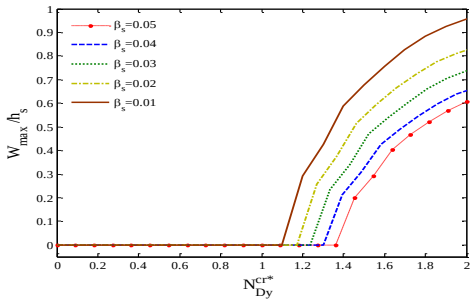

Fig. 3
Effect of shell thickness aspect ratio (β_s) on the nonlinear dynamic critical buckling load versus dimensionless transverse displacement.

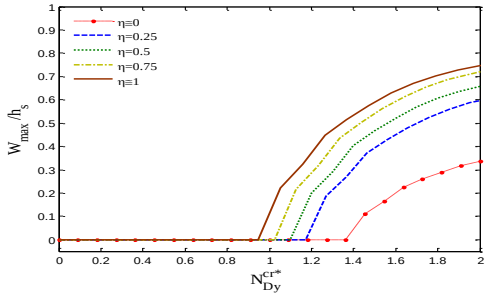

Fig. 4
Effect of core aspect ratio (η) on the nonlinear dynamic critical buckling load versus dimensionless transverse displacement.

Figs. 5 and 6 illustrate the influence of elastic medium, including Pasternak and Winkler modules, respectively on N_{Dy}^{cr*}, versus dimensionless transverse displacement. As can be seen, the elastic medium has a significant effect on nonlinear critical dynamic buckling load due to high stability of the composite shell however, for higher dimensionless spring constants, the effect of Pasternak and Winkler becomes more considerable. The higher the Winkler and Pasternak constants, the higher is the N_{Dy}^{cr*}.

In realizing the influence of material type, Fig. 7 shows how N_{Dy}^{cr*} changes versus $W_{\max}/h_s$ the shell for four different nanocomposites. For both smart matrix (PVDF) and smart reinforcement (BNNTs), the N_{Dy}^{cr*} is higher than non smart composites, i.e. when PE and CNT are used as matrix and reinforcement, respectively. This is most likely due to the fact that in piezoelectric material, the direction of polarization for both reinforcements and matrix was the same. It should be noted that effect of matrix type on dimensionless dynamic critical buckling load is higher than the nanotube type. In other word, change of matrix is very significant on N_{Dy}^{cr*} and move it very much but change the stringers (nanotube) don't have influence on the dynamic critical buckling load and just have effect on $W_{\max}/h_s$. This is perhaps because changing of nanotubs don't have effect on cylindrical shell's stiffness.

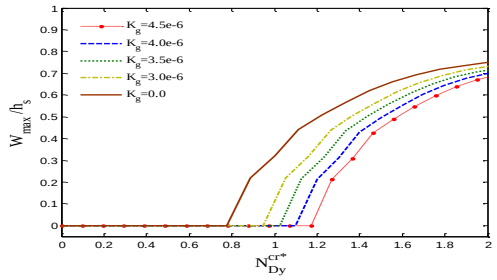

Fig. 5
Effect of Pasternak constant (K_g) on the nonlinear dynamic critical buckling load versus dimensionless transverse displacement.

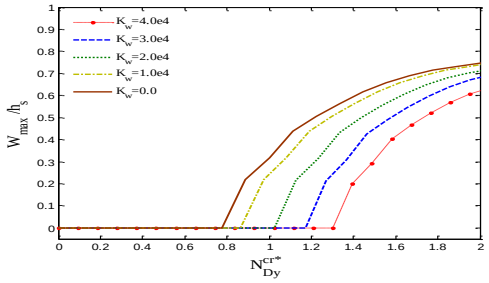

Fig. 6
Effect of Winkler constant (K_W)on the versus dimensionless transverse displacement.

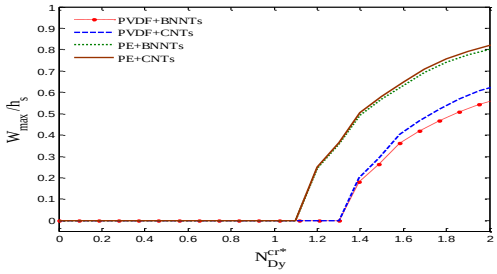

Fig. 7
The value of nonlinear dynamic critical buckling load for four different composite materials.

Fig. 8 demonstrates the influence of thermal gradient ΔT on the dynamic critical buckling load, N_{Dy}^{cr*}. Changing temperature gradients (ΔT) alters the position of critical load. It could be mentioned however, that the N_{Dy}^{cr*} decreases as ΔT is increased. The reason is that the equivalent stiffness in eigenvalue problem decreases with increasing temperature gradient. The effects of geometrical aspect ratios (i.e. γ_s and β_s) on the critical dynamic buckling load (N_{Dy}^{cr*}) versus dimensionless shell length (x/L) are illustrated in Figs. 9 and 10. It can be found that with increasing β_s and γ_s, critical dynamic buckling load increases. Furthermore, for lower shell length the geometrical aspect ratios have not significant effects on critical dynamic buckling load however, for longer shell length the effects of geometrical aspect ratios become considerable. In other words, with increasing shell length, the effects of geometrical aspect ratios on the critical dynamic buckling load become remarkable.

In the absence of similar publications in the literature covering the same scope of the problem, one can not directly validate the results found here. However, the present work could be partially validated based on a simplified analysis suggested by Mosallaie Barzoki et al. [17] on nonlinear buckling response of embedded piezoelectric cylindrical shell reinforced with BNNT in which the coefficient of dynamic load (α), PE foam-core, viscous fluid and dapping coefficient (C) in this paper were ignored. The results of validation are shown in Fig. 11 in which the dimensionless nonlinear critical buckling load (N_{NL}^{cr*}) versus shell length (x/L) is plotted for different values of dimensionless Pasternak coefficient (K_g). As can be seen the two analyses agree well and show similar results, indicating validation of our work.

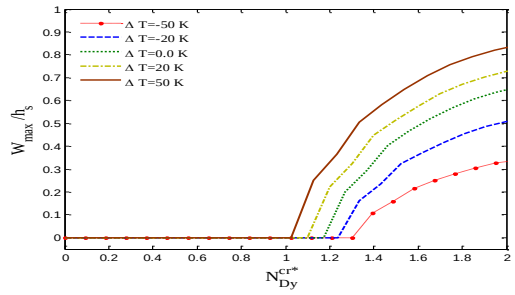

Fig. 8
Effect of thermal gradient (ΔT) on the nonlinear dynamic critical buckling load versus dimensionless transverse displacement.

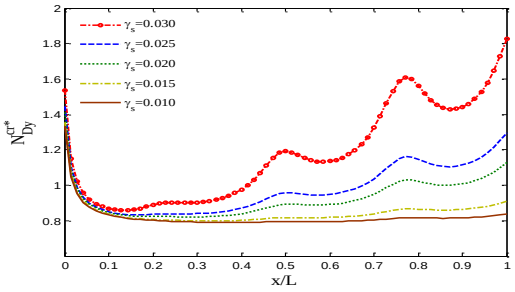

Fig. 9
Effect of shell length aspect ratio (γ_s) on the critical dynamic buckling load versus dimensionless shell length.

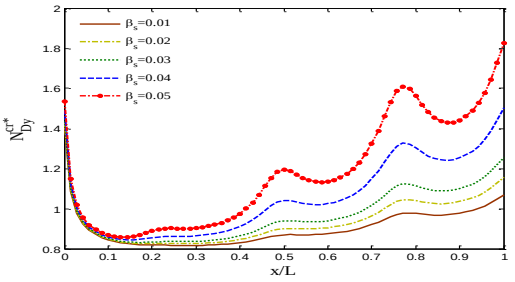

Fig. 10
Effect of shell thickness aspect ratio (β_s) on the critical dynamic buckling load versus dimensionless shell length.

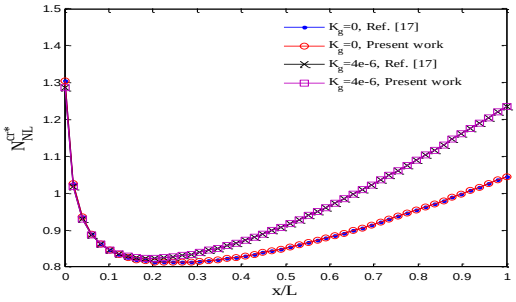

Fig. 11
Dimensionless nonlinear critical buckling load versus shell length for different values of dimensionless Pasternak coefficient.

5 CONCLUSIONS

Buckling response of PNCs conveying fluid have applications in designing many NEMS/MEMS devices such as strain sensor, mass and pressure sensors, medical fields, oil and gas as well as other high technology industries. Dynamic buckling analysis of a viscous-fluid conveying PNC cylindrical shell with foam core resting on visco-Pasternak medium was the main contribution of the present paper. Using HDQM the derived governing equations were solved to obtain the critical dynamic buckling load so that the effects of geometrical aspect ratio, in-fill ratio of core, viscoelastic medium coefficients, material types of the shell and temperature gradient were considered. Results

indicated that with increasing geometrical aspect ratio the critical dynamic buckling load of the PNC cylindrical shell increases. It was also found that the critical dynamic buckling load is decreased with increasing core thickness. Furthermore, the critical dynamic buckling load increases when piezoelectric effect is considered.

ACKNOWLEDGEMENT

The author would like to thank the reviewers for their valuable comments and suggestions to improve the clarity of this study. The authors are grateful to University of Kashan for supporting this work by Grant No. 65475/80.

APPENDIX A

$$
\begin{aligned}
&(\gamma_c\gamma_s\bar{C}_{c11}+\gamma_s^2)\left(\sum_{k=1}^{N_x}A^{(2)}{}_{ik}\bar{u}(x_k,\theta_j)+\sum_{k=1}^{N_x}A^{(1)}{}_{ik}\bar{w}(x_k,\theta_j)\sum_{k=1}^{N_x}A^{(2)}{}_{ik}\bar{w}(x_k,\theta_j)\right)\\
&+\frac{\beta_c\gamma_s\bar{C}_{c12}}{\eta}\left(\sum_{k=1}^{N_x}\sum_{p=1}^{N_\theta}A^{(1)}{}_{ik}B^{(1)}{}_{jp}\bar{w}(x_k,\theta_j)+\sum_{k=1}^{N_x}A^{(1)}{}_{ik}\bar{w}(x_k,\theta_j)\right.\\
&\left.\frac{\beta_c}{\eta}\sum_{p=1}^{N_\theta}B^{(1)}{}_{jp}\bar{w}(x_k,\theta_j)\sum_{k=1}^{N_x}\sum_{p=1}^{N_\theta}A^{(1)}{}_{ik}B^{(1)}{}_{jp}\bar{w}(x_k,\theta_j)\right)+\gamma_s\beta_s\bar{C}_{s12}\left(\sum_{k=1}^{N_x}\sum_{p=1}^{N_\theta}A^{(1)}{}_{ik}B^{(1)}{}_{jp}\bar{v}(x_k,\theta_j)+\sum_{k=1}^{N_x}A^{(1)}{}_{ik}\bar{w}(x_k,\theta_j)\right.\\
&\left.\beta_s\sum_{p=1}^{N_\theta}B^{(1)}{}_{jp}\bar{w}(x_k,\theta_j)\sum_{k=1}^{N_x}\sum_{p=1}^{N_\theta}A^{(1)}{}_{ik}B^{(1)}{}_{jp}\bar{w}(x_k,\theta_j)\right)+\frac{\beta_c^2\gamma_s\bar{C}_{c66}}{\eta^2}\left(\sum_{p=1}^{N_\theta}B^{(2)}{}_{jp}\bar{u}(x_k,\theta_j)+\frac{\eta}{\beta_c}\sum_{k=1}^{N_x}\sum_{p=1}^{N_\theta}A^{(1)}{}_{ik}B^{(1)}{}_{jp}\bar{v}(x_k,\theta_j)\right.\\
&\left.+\sum_{k=1}^{N_x}A^{(1)}{}_{ik}\bar{w}(x_k,\theta_j)\sum_{p=1}^{N_\theta}B^{(2)}{}_{jp}\bar{w}(x_k,\theta_j)+\frac{\eta}{\beta_c}\sum_{k=1}^{N_x}A^{(1)}{}_{ik}\bar{w}(x_k,\theta_j)+\sum_{p=1}^{N_\theta}B^{(1)}{}_{jp}\bar{w}(x_k,\theta_j)\sum_{k=1}^{N_x}\sum_{p=1}^{N_\theta}A^{(1)}{}_{ik}B^{(1)}{}_{jp}\bar{v}(x_k,\theta_j)\right)\\
&+\beta_s\bar{C}_{s66}\left(\beta_s\sum_{p=1}^{N_\theta}B^{(2)}{}_{jp}\bar{u}(x_k,\theta_j)+\sum_{k=1}^{N_x}\sum_{p=1}^{N_\theta}A^{(1)}{}_{ik}B^{(1)}{}_{jp}\bar{v}(x_k,\theta_j)+\beta_s\sum_{k=1}^{N_x}A^{(1)}{}_{ik}\bar{w}(x_k,\theta_j)\sum_{p=1}^{N_\theta}B^{(2)}{}_{jp}\bar{u}(x_k,\theta_j)+\sum_{k=1}^{N_x}A^{(1)}{}_{ik}\bar{w}(x_k,\theta_j)\right.\\
&\left.+\beta_s\sum_{p=1}^{N_\theta}B^{(1)}{}_{jp}\bar{w}(x_k,\theta_j)\sum_{k=1}^{N_x}\sum_{p=1}^{N_\theta}A^{(1)}{}_{ik}B^{(1)}{}_{jp}\bar{v}(x_k,\theta_j)\right)+\bar{e}_{c11}\sum_{k=1}^{N_x}A^{(2)}{}_{ik}\Phi(x_k,\theta_j)=C\dot{\bar{u}}(x_k,\theta_j)+\left(\bar{\rho}_c\frac{\beta_c}{\beta_s}+\bar{\rho}_s\right)\ddot{\bar{u}}(x_k,\theta_j)
\end{aligned}
\tag{A.1}
$$

$$
\begin{aligned}
&\frac{\beta_c\bar{C}_{c12}}{\eta}\left(\sum_{k=1}^{N_x}\sum_{p=1}^{N_\theta}A^{(1)}{}_{ik}B^{(1)}{}_{jp}\bar{u}(x_k,\theta_j)+\sum_{k=1}^{N_x}A^{(1)}{}_{ik}\bar{w}(x_k,\theta_j)\right.\\
&\left.\sum_{k=1}^{N_x}\sum_{p=1}^{N_\theta}A^{(1)}{}_{ik}B^{(1)}{}_{jp}\bar{w}(x_k,\theta_j)\right)+\beta_s\bar{C}_{s12}\left(\sum_{k=1}^{N_x}\sum_{p=1}^{N_\theta}A^{(1)}{}_{ik}B^{(1)}{}_{jp}\bar{u}(x_k,\theta_j)+\sum_{k=1}^{N_x}A^{(1)}{}_{ik}\bar{w}(x_k,\theta_j)\sum_{k=1}^{N_x}\sum_{p=1}^{N_\theta}A^{(1)}{}_{ik}B^{(1)}{}_{jp}\bar{w}(x_k,\theta_j)\right)\\
&+\frac{\beta_c\beta_s\bar{C}_{c22}}{\eta^2}\left(\sum_{p=1}^{N_\theta}B^{(2)}{}_{jp}\bar{v}(x_k,\theta_j)+\sum_{p=1}^{N_\theta}B^{(1)}{}_{jp}\bar{w}(x_k,\theta_j)+\frac{\beta_c}{\eta}\sum_{p=1}^{N_\theta}B^{(1)}{}_{jp}\bar{w}(x_k,\theta_j)\sum_{p=1}^{N_\theta}B^{(2)}{}_{jp}\bar{w}(x_k,\theta_j)\right)\\
&+\beta_s^2\bar{C}_{s22}\left(\sum_{p=1}^{N_\theta}B^{(2)}{}_{jp}\bar{v}(x_k,\theta_j)+\sum_{p=1}^{N_\theta}B^{(1)}{}_{jp}\bar{w}(x_k,\theta_j)+\beta_s\sum_{p=1}^{N_\theta}B^{(1)}{}_{jp}\bar{w}(x_k,\theta_j)\sum_{p=1}^{N_\theta}B^{(2)}{}_{jp}\bar{w}(x_k,\theta_j)\right)\\
&+\frac{\beta_c\gamma_c\bar{C}_{c66}}{\eta}\left(\sum_{k=1}^{N_x}\sum_{p=1}^{N_\theta}A^{(1)}{}_{ik}B^{(1)}{}_{jp}\bar{u}(x_k,\theta_j)+\frac{\eta}{\beta_c}\sum_{k=1}^{N_x}A^{(2)}{}_{ik}\bar{v}(x_k,\theta_j)+\sum_{k=1}^{N_x}\sum_{p=1}^{N_\theta}A^{(1)}{}_{ik}B^{(1)}{}_{jp}\bar{w}(x_k,\theta_j)\sum_{k=1}^{N_x}A^{(1)}{}_{ik}\bar{w}(x_k,\theta_j)\right.\\
&\left.+\sum_{p=1}^{N_\theta}B^{(1)}{}_{jp}\bar{w}(x_k,\theta_j)\sum_{k=1}^{N_x}A^{(2)}{}_{ik}\bar{w}(x_k,\theta_j)\right)+\gamma_s\bar{C}_{s66}\left(\beta_s\sum_{k=1}^{N_x}\sum_{p=1}^{N_\theta}A^{(1)}{}_{ik}B^{(1)}{}_{jp}\bar{u}(x_k,\theta_j)+\sum_{k=1}^{N_x}A^{(2)}{}_{ik}\bar{v}(x_k,\theta_j)\right.\\
&\left.+\beta_s\sum_{k=1}^{N_x}\sum_{p=1}^{N_\theta}A^{(1)}{}_{ik}B^{(1)}{}_{jp}\bar{w}(x_k,\theta_j)\sum_{k=1}^{N_x}A^{(1)}{}_{ik}\bar{w}(x_k,\theta_j)+\beta_s\sum_{p=1}^{N_\theta}B^{(1)}{}_{jp}\bar{w}(x_k,\theta_j)\sum_{k=1}^{N_x}A^{(2)}{}_{ik}\bar{w}(x_k,\theta_j)\right)\\
&=C\dot{\bar{v}}(x_k,\theta_j)+\left(\bar{\rho}_c\frac{\beta_c}{\beta_s}+\bar{\rho}_s\right)\ddot{\bar{v}}(x_k,\theta_j)
\end{aligned}
\tag{A.2}
$$

$$
\begin{aligned}
&\frac{\gamma_s^2}{12}\left(-\gamma_s^2\sum_{k=1}^{N_x}A^{(4)}{}_{ik}\,\overline{w}(x_k,\theta_j)-\overline{C}_{s12}\beta_s^2\sum_{k=1}^{N_x}\sum_{p=1}^{N_\theta}A^{(2)}{}_{ik}B^{(2)}{}_{jp}\,\overline{w}(x_k,\theta_j)\right)\\
&+\frac{1}{12}\left(-\gamma_s^2\beta_s^2\overline{C}_{s12}\sum_{k=1}^{N_x}\sum_{p=1}^{N_\theta}A^{(2)}{}_{ik}B^{(2)}{}_{jp}\,\overline{w}(x_k,\theta_j)-\beta_s^4\overline{C}_{s22}\sum_{p=1}^{N_\theta}B^{(4)}{}_{jp}\,\overline{w}(x_k,\theta_j)\right)\\
&-\frac{\gamma_s^2\beta_s^2\overline{C}_{c66}}{3}\left(\sum_{k=1}^{N_x}\sum_{p=1}^{N_\theta}A^{(2)}{}_{ik}B^{(2)}{}_{jp}\,\overline{w}(x_k,\theta_j)\right)-\left(\frac{\gamma_c\beta_c C_{c12}}{3\eta}+\frac{\gamma_s\beta_s\overline{C}_{s12}}{3}\right)\\
&\left(\sum_{k=1}^{N_x}A^{(1)}{}_{ik}\,\overline{u}(x_k,\theta_j)+\frac{\gamma_s}{2}\sum_{k=1}^{N_x}A^{(1)}{}_{ik}\,\overline{w}(x_k,\theta_j)\sum_{k=1}^{N_x}A^{(1)}{}_{ik}\,\overline{w}(x_k,\theta_j)\right)\\
&-\left(\frac{\gamma_c\beta_c\overline{C}_{c22}}{\eta}\right)\left(\sum_{p=1}^{N_\theta}B^{(1)}{}_{jp}\,\overline{v}(x_k,\theta_j)+\frac{\gamma_s\,\overline{w}(x_k,\theta_j)}{\eta}+\frac{1}{2}\frac{\beta_s^2}{\eta^2}\sum_{p=1}^{N_\theta}B^{(1)}{}_{jp}\,\overline{w}(x_k,\theta_j)\right.\\
&\left.\sum_{p=1}^{N_\theta}B^{(1)}{}_{jp}\,\overline{w}(x_k,\theta_j)\right)-\beta_s\overline{C}_{s22}\left(\sum_{p=1}^{N_\theta}B^{(1)}{}_{jp}\,\overline{v}(x_k,\theta_j)+\beta_s\,\overline{w}(x_k,\theta_j)+\frac{\beta_s^2}{2}\sum_{p=1}^{N_\theta}B^{(1)}{}_{jp}\,\overline{w}(x_k,\theta_j)\sum_{p=1}^{N_\theta}B^{(1)}{}_{jp}\,\overline{w}(x_k,\theta_j)\right)\\
&-\frac{\beta_c\overline{C}_{c22}}{\eta}\left(\sum_{p=1}^{N_\theta}B^{(1)}{}_{jp}\,\overline{v}(x_k,\theta_j)+\frac{\beta_s\overline{w}(x_k,\theta_j)}{\eta}+\frac{\beta_s^2}{2\eta^2}\sum_{p=1}^{N_\theta}B^{(1)}{}_{jp}\,\overline{w}(x_k,\theta_j)\sum_{p=1}^{N_\theta}B^{(1)}{}_{jp}\,\overline{w}(x_k,\theta_j)\right)\\
&-\left(\left(\beta_s^2\,\alpha_{xs}+\frac{\beta_s\beta_c\overline{C}_{c11}\,\alpha_{xc}}{\eta^2}+\beta_s^2\,\overline{C}_{s12}\,\alpha_{\theta s}+\frac{\beta_s\beta_c\overline{C}_{c12}\,\alpha_{\theta c}}{\eta^2}\right)\Delta T\sum_{p=1}^{N_\theta}B^{(2)}{}_{jp}\,\overline{w}(x_k,\theta_j)\right.\\
&\left.-\left(\gamma_s^2\,\alpha_{xs}+\gamma_c\gamma_s\overline{C}_{c11}\,\alpha_{xc}+\gamma_s^2\overline{C}_{s12}\,\alpha_{\theta s}+\gamma_c\gamma_s\overline{C}_{c12}\,\alpha_{\theta c}\right)\sum_{k=1}^{N_x}A^{(2)}{}_{ik}\,\overline{w}(x_k,\theta_j)\right)\Delta T\\
&-\left[\frac{\beta_c}{\beta_s}\ddot{\overline{w}}(x_k,\theta_j)+2\,\gamma_c V\sum_{k=1}^{N_x}A^{(1)}{}_{ik}\dot{\overline{w}}(x_k,\theta_j)+\gamma_c\gamma_s V^2\sum_{k=1}^{N_x}A^{(2)}{}_{ik}\,\overline{w}(x_k,\theta_j)\right]\\
&-\overline{\mu}\,\gamma_c\gamma_s\left[\sum_{k=1}^{N_x}A^{(2)}{}_{ik}\,\dot{\overline{w}}(x_k,\theta_j)+V\gamma_s^2\gamma_c\sum_{k=1}^{N_x}A^{(3)}{}_{ik}\,\overline{w}(x_k,\theta_j)+\frac{\beta_s\beta_c}{\eta^2}\left(\sum_{p=1}^{N_\theta}B^{(2)}{}_{jp}\dot{\overline{w}}(x_k,\theta_j)+V\gamma_s\sum_{k=1}^{N_x}\sum_{p=1}^{N_\theta}A^{(1)}{}_{ik}B^{(2)}{}_{jp}\,\overline{w}(x_k,\theta_j)\right)\right]\\
&-\left(K_{gs}+K_{gc}\right)\left(\gamma_s^2\sum_{k=1}^{N_x}A^{(2)}{}_{ik}\,\overline{w}(x_k,\theta_j)+\beta_s^2\sum_{p=1}^{N_\theta}B^{(2)}{}_{jp}\,\overline{w}(x_k,\theta_j)\right)\\
&+\left(K_{ws}+K_{wc}\right)\overline{w}(x_k,\theta_j)+\gamma_s N_{x0}^*\sum_{k=1}^{N_x}A^{(2)}{}_{ik}\,\overline{w}(x_k,\theta_j)=C\,\dot{\overline{w}}(x_k,\theta_j)+\left(\overline{\rho}_c\frac{\beta_c}{\beta_s}+\overline{\rho}_s\right)\ddot{\overline{w}}(x_k,\theta_j)
\end{aligned}
\tag{A.3}
$$

$$
-\sum_{k=1}^{N_x}A^{(2)}{}_{ik}\Phi(x_k,\theta_j)+\overline{e}_{11}\sum_{k=1}^{N_x}A^{(2)}{}_{ik}\overline{u}(x_k,\theta_j)+\gamma_c\sum_{k=1}^{N_x}A^{(1)}{}_{ik}\overline{w}(x_k,\theta_j)\sum_{k=1}^{N_x}A^{(2)}{}_{ik}\overline{w}(x_k,\theta_j)=0 \tag{A.4}
$$

REFERENCES

[1] Kim S.E., Kim Ch.S., 2002, Buckling strength of the cylindrical shell and tank subjected to axially compressive loads, *Thin-Walled Structures* **40**:329-353.

[2] Ghorbanpour Arani A., Golabi S., Loghman A., Daneshi H., 2007, Investigating elastic stability of cylindrical shell with an elastic core under axial compression by energy method, *Journal of Mechanical Science and Technology* **21**:693-698.

[3] Ghorbanpour Arani A., Loghman A., Mosallaie Barzoki A.A., Kolahchi R., 2011, Elastic buckling analysis of ring and stringer-stiffened cylindrical shells under general pressure and axial compression via the Ritz method, *Journal of Solid Mechanics* **1**:332-347.

[4] Das P.K., Thavalingam A., Bai Y., 2003, Buckling and ultimate strength criteria of stiffened shells under combined loading for reliability analysis, *Thin-Walled Structures* **41**:69-88.

[5] Hubner A., Albiez M., Kohler D., Saal H., 2007, Buckling of long steel cylindrical shells subjected to external pressure, *Thin-Walled Structures* **45**:1-7.

[6] Patel S.N., Datta P.K., Sheikh A.H. 2006, Buckling and dynamic instability analysis of stiffened shell panels, *Thin-Walled Structures* **44**:321-333.

[7] Huang H., Han Q., 2010, Nonlinear dynamic buckling of functionally graded cylindrical shells subjected to time-dependent axial load, *Composite Structures* **92**:593-598.

[8] Bisagni C.H., 2005, Dynamic buckling of fiber composite shells under impulsive axial compression, *Thin-Walled Structures* **43**:499-514.
[9] Shariyat M., 2010, Non-linear dynamic thermo-mechanical buckling analysis of the imperfect sandwich plates based on a generalized three-dimensional high-order global–local plate theory, *Composite Structures* **92**:72-85.
[10] Wan H., Delale F., Shen L., 2005, Effect of CNT length and CNT-matrix interphase in carbon nanotube (CNT) reinforced composites, *Mechanics Research Communication* **32**:481-489.
[11] Li K., Saigal S., 2007, Micromechanical modeling of stress transfer in carbon nanotube reinforced polymer composites, *Materials Science Engineering A* **457**:44-57.
[12] Han S.C.H., Tabiei A., Park W.T., 2008, Geometrically nonlinear analysis of laminated composite thin shells using a modified first-order shear deformable element-based Lagrangian shell element, *Composite Structures* **82**:465-474.
[13] Wang X., 2007, Nonlinear stability analysis of thin doubly curved orthotropic shallow shells by the differential quadrature method, *Computer Methods in Applied Mechanics and Engineering* **196**:2242-2251.
[14] Haftchenari H., Darvizeh M., Darvizeh A., Ansari R., Sharma C.B., 2007, Dynamic analysis of composite cylindrical shells using differential quadrature method (DQM), *Composite Structures* **78**:292-298.
[15] Alibeigloo A., 2009, Static and vibration analysis of axi-symmetric angle-ply laminated cylindrical shell using state space differential quadrature method, *International Journal of Pressure and Vessel and Piping* **86**:738-747.
[16] Mosallaie Barzoki A.A., Ghorbanpour Arani A., Kolahchi R., Mozdianfard M.R., 2012, Electro-thermo-mechanical torsional buckling of a piezoelectric polymeric cylindrical shell reinforced by DWBNNTs with an elastic core, *Applied Mathematical Modelling* **36**:2983-2995.
[17] Mosallaie Barzoki A.A., Ghorbanpour Arani A., Kolahchi R., Mozdianfard M.R., Loghman A., 2013, Nonlinear buckling response of embedded piezoelectric cylindrical shell reinforced with BNNT under electro–thermo-mechanical loadings using HDQM, *Composite Part B: Engineering* **44**:722-727.
[18] Ghorbanpour Arani A., Kolahchi R., Mosallaie Barzoki A.A., 2011, Effect of material inhomogeneity on electro-thermo-mechanical behaviors of functionally graded piezoelectric rotating cylinder, *Applied Mathematical Modelling* **35**:2771-2789.
[19] Ghorbanpour Arani A., Kolahchi R., Mosallaie Barzoki A.A., Loghman A., 2012, Electro-thermo-mechanical behaviors of FGPM spheres using analytical method and ANSYS software, *Applied Mathematical Modelling* **36**:139-157.
[20] Ghorbanpour Arani A., Mosallaie Barzoki A.A, Kolahchi R., Mozdianfard M.R., Loghman A., 2011, Semi-analytical solution of time-dependent electro-thermo-mechanical creep for radially polarized piezoelectric cylinder, *Computers and Structures* **89**: 1494-1502.
[21] Amabili M. 2008, *Nonlinear Vibrations and Stability of Shells and Plates*, Cambridge University Press, New York.
[22] Liew K.M., Han J.B., Xiao Z.M., 1996, Differential quadrature method for thick symmetric cross-ply laminates with first-order shear flexibility, *International Journal of Solids and Structures* **33**:2647-2658.
[23] Civalek Ö., 2004, Application of differential quadrature (DQ) and harmonic differential quadrature (HDQ) for buckling analysis of thin isotropic plates and elastic columns, *Engineering Structures* **26**:171-186.
[24] Abdollahian M., Ghorbanpour Arani A., Mosallaie Barzoki A.A., Kolahchi R., Loghman A., 2013, Non-local wave propagation in embedded armchair TWBNNTs conveying viscous fluid using DQM, *Physica B* **418**:1-15.